Contents lists available at SciVerse ScienceDirect

Tectonophysics

journal homepage: www.elsevier.com/locate/tecto

Effects of a revised rate- and state-dependent friction law on aftershock triggering model

Nobuki Kame *, Satoshi Fujita, Masao Nakatani, Tetsuya Kusakabe

Earthquake Research Institute, the University of Tokyo, 1-1-1 Yayoi, Bunkyo-ku, Tokyo 113-0032, Japan

ARTICLE INFO

ABSTRACT

Seismicity may be considered as a sequence of earthquake nucleation events controlled by regional loading history. On the basis of this concept, Dieterich (1994) modeled aftershock seismicity following an imposed stress step, by using a laboratory-derived rate- and state-dependent friction law (RSF). Although this model predicts the canonical $1/t$ decay of aftershock rate, two huge gaps from observations are known; the model, with frictional parameters assumed to be laboratory-observed values, predicts too low aftershock productivity and also too long a delay before the decay onset. These gaps are by orders of magnitude. We suspected that the problem might be the incorrectness of traditional RSFs, none of which was free from contradictions with laboratory data. Hence we modeled aftershock triggering with a revised RSF (Nagata et al., 2012), which seems to have resolved the previously known flaws in reproducing laboratory data. The original analytic approach of Dieterich (1994) was found invalid for the revised RSF, so we did an equivalent analysis by numerically tracking individual nucleation sources. The revised RSF produced generally similar aftershock seismicity, with the gaps mentioned above narrowed by a factor, though these are far too small improvements of the huge gaps, that is, the revised RSF did not fully resolve the problem. On the other hand, our simulations found a counterintuitive response of a fault obeying the revised RSF; if imposed during a certain stage in the seismic cycle, a positive stress step can cause oscillatory slow slip events before eventual seismic instability, instead of a usual response of further monotonic acceleration to seismic instability. This delays the timing of the next earthquake. Due to this behavior, the exponent of the aftershock decay can be greater than unity. Also, the decay can once overshoot below the background seismicity before eventually returning to the background level.

© 2012 Elsevier B.V. All rights reserved.

1. Introduction

Rate- and state-dependent friction law (RSF), introduced by Dieterich (1979) on the basis of laboratory friction experiments, has been used to model a wide spectrum of earthquake behaviors, successfully explaining the mechanics of seismic cycles (e.g., Tse and Rice, 1986), episodic aseismic slips (e.g., Yoshida and Kato, 2003), triggered seismicity (e.g., Dieterich, 1994) and many others. In the present paper, we turn our attention to the modeling of aftershock seismicity, the major part of earthquake clustering, focusing on the effects of frictional properties.

Dieterich (1994) modeled seismicity as a sequence of earthquake nucleation events, where the timing of each earthquake was controlled by the stressing history and the distribution of initial conditions over the population of nucleation sources, the concept we follow in this paper. To implement this concept, a specific model of the earthquake nucleation process is necessary and "time to instability analysis" obeying RSF (Dieterich, 1992) was chosen for this

purpose. The analysis gives the time to instability t_i of each receiver fault as a function of the imposed stress step loading $\Delta\tau$ and the initial condition of the fault that can be specified with the slip velocity V_0 just before the step loading. This analysis is then applied to a population of receiver faults with a distribution of initial conditions calibrated so that a reference seismicity rate r is realized under a constant stressing rate $\dot{\tau}_r$. This then allows theoretical prediction of seismicity for a given history of the regional stress field, and the seismicity following a stress step caused by a mainshock can be specifically regarded as an aftershock sequence.

The predicted aftershock rate $R(t)$ following a stress step $\Delta\tau$ at $t = 0$ has the form of Omori–Utsu law $R = R_0(1 + t/t_e)^{-p}$ (Omori, 1894; Utsu, 1961) for $t/t_a < 1$ with the exponent $p = 1$, but it merges to the background rate r for $t/t_a > 1$. Here $R_0 (= R(0))$ is the initial aftershock rate, t_e is the onset of time decay and t_a is the aftershock duration (Fig. 1). According to the model, these three observable quantities strongly depend on the product of the effective normal stress $\sigma_e (= \sigma - P$, $\sigma =$ fault normal stress, $P =$ pore pressure) and a (a nondimensional positive RSF parameter called direct effect coefficient). Specifically, $R_0 = r\exp(\Delta\tau/(a\sigma_e))$, $t_e = t_a\exp(-\Delta\tau/(a\sigma_e))$ and $t_a = a\sigma_e/\dot{\tau}_r$.

* Corresponding author. Tel.: +81 3 5841 5694; fax: +81 3 5802 3391.
E-mail address: kame@eri.u-tokyo.ac.jp (N. Kame).
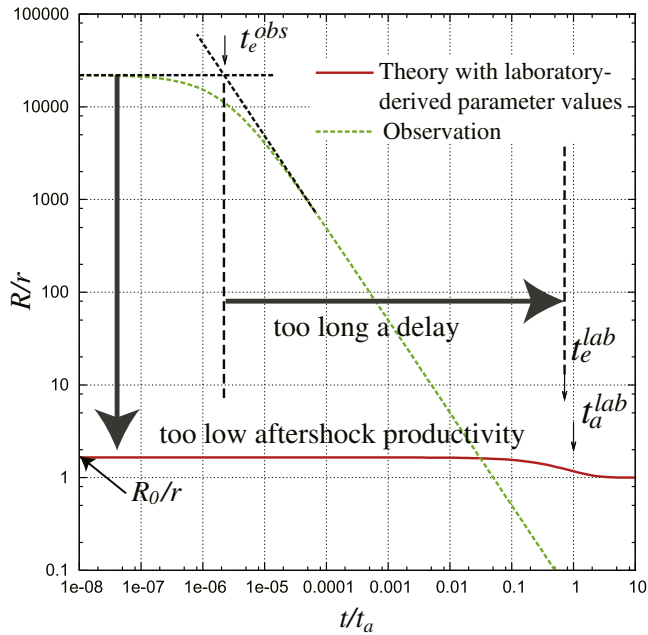
Fig. 1. Comparison of normalized aftershock seismicity R/r between theory (solid line) and typical observation (dashed line). For a given stress step $\Delta\tau = 0.5$ MPa, the theory with laboratory-derived parameters $a\sigma_e = 1.0$ MPa (solid line) predicts too low aftershock productivity and too long a delay of the onset of time decay, compared to observation (dashed line). Typical observation requires much smaller $a\sigma_e$ values to be fitted with the theory (the dashed line shown here corresponds to $a\sigma_e = 0.05$ MPa). Theoretical predictions are as follows: the initial rate $R_0 = r\exp(\Delta\tau/(a\sigma_e))$, onset of time decay $t_e = t_a\exp(-\Delta\tau/(a\sigma_e))$, aftershock duration $t_a = a\sigma_e/\dot\tau_r$ and $1/t$ time decay between $t_e < t < t_a$.

The Dieterich (1994) model is based only on very general assumptions, so comparison with observation has been made for various aftershock cases (e.g., Dieterich, 1994; Gross and Kisslinger, 1994; Toda et al., 1998) as well as for cases involving other trigger forces including seismic wave (Gomberg et al., 1998), postseismic slip or transient deformation related with intrusions or eruptions (Dieterich et al., 2000), slow earthquakes (Lohman and McGuire, 2007; Segall et al., 2006) or tides (Cochran et al., 2004). The Dieterich (1994) model shows two major quantitative gaps from most aftershock sequences. One is too low aftershock productivity and the other is too long a delay t_e before the decay onset (Fig. 1). When interpreting an aftershock sequence, $\dot\tau_r$, r, and $\Delta\tau$ are directly constrained by observations, and the only adjustable model parameter is $a\sigma_e$ of receiver faults (e.g., Toda et al., 1998). With a consensual value of $a = 0.01$ from laboratory (Marone, 1995) and a representative value of $\sigma_e = 100$ MPa at a seismogenic depth of 10 km (which corresponds to P in the midway between hydrostatic and lithostatic values), $a\sigma_e$ is approximately 1 MPa. For a reasonable range of stress step from $\Delta\tau = 0.01$ to 1 MPa, this characteristic stress of $a\sigma_e = 1$ MPa predicts too small R_0 and too large t_e, differing from most observations by many orders of magnitude (Fig. 1). Much smaller $a\sigma_e$ is usually required to match the observed aftershock seismicity. For example, Toda et al. (2005) had to adopt $a\sigma_e = 0.05$ MPa to fit the observed seismicity in the eastern California. This problem is noticed in virtually every study that has attempted to match aftershocks with the Dieterich model (Dieterich, 1994; Toda et al., 1998).

A commonly proposed resolution is to assume a nearly zero σ_e, that is, a nearly lithostatic pore pressure. Considering that high R_0 and short t_e are observed for most aftershock sequences across different tectonic settings (e.g., Dieterich, 1994), this resolution implies that a nearly lithostatic pore pressure is a norm across various seismogenic environments, whereas the earth's permeable crust does not readily allow such a high pore pressure (Scholz, 2002). So, we wish to find other resolutions.

We suspect that the problem may be the RSF itself. The use of RSF for fault mechanics modeling is justified because it is based on laboratory rock friction experiments. However, it has been long recognized that RSF has clear shortcomings in reproducing laboratory results (e.g., Kato and Tullis, 2001; Marone, 1995). Several different formulae have been proposed to overcome the problem, but none of them were free from some drawbacks that contradict laboratory data in some aspects (e.g., Nakatani, 2001) until Nagata et al. (2012) came up with a fairly drastic revision. The present paper looks for implications of this revised RSF (called the Nagata RSF hereafter) on Dieterich's (1994) aftershock triggering model.

Subtle differences in RSF formulae sometimes lead to important consequences in modeled fault behaviors. For example, simulations of earthquake nucleation in an elastic continuum show that different evolution laws may lead to qualitatively different nucleation patterns (Ampuero and Rubin, 2008). In the present paper, we model the aftershock triggering using the Nagata RSF that seems to have resolved the previously known flaws in reproducing laboratory data. Differences made by Nagata RSF will be elucidated by comparison with the results based on the "slowness" version of traditional RSF, which is the direct predecessor of the Nagata RSF.

2. Background: The revised RSF

We briefly summarize the revised RSF, which has been recently tried in simulations of earthquake cycle (Kame et al., 2013) and earthquake nucleation in elastic continuum (Kame et al., in preparation). Nagata et al. (2012) obtained the revised RSF by constraining constitutive law and evolution law separately with laboratory data. The constitutive law describes the relationship between applied shear stress and slip velocity as

$$V = V_* \exp\left\{\frac{\tau - \Phi}{a\sigma_e}\right\}, \quad \text{or} \quad \tau = \Phi + a\sigma_e \ln\left(\frac{V}{V_*}\right), \tag{1}$$

where τ is the shear stress, V is the slip velocity, V_* is an arbitrarily chosen reference velocity, and Φ is the state variable specifying the internal physical state of the interface, which, in many cases, may correspond to the real contact area (e.g., Dieterich and Kilgore, 1996). In the revised RSF, the direct effect coefficient a was constrained to be as large as 0.05, about five times larger than traditionally believed. The difference came from that they could constrain the direct effect without using any evolution laws, contrasting to earlier studies where imperfection of real-world "step" tests was corrected for by use of some presumed evolution law. The large a immediately leads to a five times larger $b \sim 0.05$ as well because $(b - a) \sim 0$ is directly constrained from the experiments without ambiguity.

The other half of RSF is the evolution law describing the variations of the state Φ for various reasons. One popular version of the evolution law, called the slowness law or the Dieterich law (e.g., Beeler et al., 1994) is written as

$$\frac{d\Phi}{dt} = \frac{b\sigma_e}{L} V_* \exp\left[-\frac{\Phi - \Phi_*}{b\sigma_e}\right] - \frac{b\sigma_e}{L} V, \tag{2}$$

where L is a characteristic length dimension and Φ_* is a reference state. The first term of Eq. (2) represents logarithmic time-dependent healing, while the second term represents linear slip weakening at a constant rate b/L per unit slip independent of the state (Nakatani, 2001). The Dieterich law explains time-healing data very well but has trouble in reproducing the change of friction over a fixed characteristic slip distance as observed (Kato and Tullis, 2001; Nakatani, 2001; Ruina, 1983; Weeks, 1993). Following the revision of the constitutive law, Nagata et al. (2012) analyzed the difference between $\Phi = \tau - a\sigma_e \ln(V/V_*)$ calculated from the measured (V, τ, σ_e) with the correct a-value and the predicted Φ by the slowness

version of evolution law (Eq. 2) with the measured slip history substituted to it. The revealed misprediction in $\dot{\Phi}$ was a function of $\dot{\tau}$ with a strong linear negative dependence. The revised evolution law was accordingly proposed as

$$\frac{d\Phi}{dt} = \frac{b\sigma_e}{L}V_* exp\left[-\frac{\Phi - \Phi_*}{b\sigma_e}\right] - \frac{b\sigma_e}{L}V - c\frac{d\tau}{dt}, \qquad (3)$$

where c is a positive coefficient of the stress-weakening effect and was determined to be about 2.0 from the above misprediction analysis. They speculated that the stress-weakening effect involved elastic tilting of the asperities that would tear some junction bonds.

Nagata et al. (2012) derived significantly different frictional parameter sets in fitting their velocity-step data (called data N hereafter) with the original (Dieterich) RSF and with the revised (Nagata) RSF. Here the Dieterich RSF means Eq. (1) with the traditional a-value and Eq. (2), while the Nagata RSF means Eq. (1) with the revised a-value and Eq. (3). The parameter sets are N-0: $(a, b, c, L) =$ (0.017, 0.0225, 0.0, 0.62 μm) for the Dieterich RSF and N-2: $(a, b, c, L) =$ (0.051, 0.0565, 2.0, 0.33 μm) for the Nagata RSF, where N stands for "data N" and "0" or "-2" refers to the c-value. Note that setting $c = 0$ in Eq. (3) leads to Eq. (2). Quantities are denoted with superscript "D" for N-0 and "N" for N-2 in the below. It is worth noticing that values of a^D and $a^N/(c + 1)$ are similar when they are obtained by the fitting of the same velocity-step data.

Reproduction of shear stress was fine with either RSF because parameters were adjusted to fit the shear stress data. However, note that the Nagata RSF could reproduce both τ and V well whereas the original RSF mispredicted V (Kame et al., 2013). This suggests that the specific nucleation process obeying the original RSF might have been wrongly inferred. This is one motivation to reconstruct the aftershock model of Dieterich (1994) with the Nagata RSF. In addition, we note that the gaps from the observation mentioned earlier are in the sense that the theoretical prediction is "less brittle (too much interval between the main shock and the triggered events)" than the observed aftershock sequences. The Nagata RSF seems to have an edge with its brittle features such as "stress weakening" and "high rate of slip weakening b^N/L^N," though "large a^N" may rather represent ductility. In the following, we construct an aftershock triggering model considering faults obeying the Nagata RSF.

3. Aftershock model with RSF

We first summarize the original analytic approach of Dieterich (1994) in Section 3.1. In Section 3.2, we show that his elegant approach can not be directly applied to the case with the revised RSF where the time-healing term is not safely omitted. We hence employ an equivalent numerical approach (Section 3.3) where each nucleation source is tracked by solving full RSF equations. In reviewing the results from our numeric approach, we noticed that another fundamental approximation made in Dieterich's (1994) analytic approach is severely violated for the Nagata RSF. This will be discussed in Section 4 when we show our model results.

3.1. Original analytic approach

Dieterich (1994) derived aftershock rate $R(t)$ following a stress step $\Delta\tau$ in an analytic closed form. It is based on a specific simplified nucleation model derived by "time to instability" analysis (Dieterich, 1992) as reviewed below. The nucleation model considers a fault patch of a fixed dimension embedded in an elastic body. The conditions along the fault are represented by the center-point values and the patch has an effective stiffness k. Equating the constitutive law Eq. (1) with the fault stress gives

$$\tau_r(t) - k\delta = \Phi + a\sigma_e ln(V/V_*), \qquad (4)$$

where $\tau_r(t)$ is the remotely applied stress acting on the fault in the absence of slip δ, and $-k\delta$ is the decrease in stress due to fault slip. Eq. (4), coupled with the evolution law Eq. (2), can be solved numerically. However, in the nucleation stage where the slip velocity is much greater than the steady-state velocity, the first time-healing term in Eq. (2) may be negligible. If the remote loading is at a constant rate as $\tau_r(t) = \tau_0 + \dot{\tau}_r t$, the simplified equation has the following analytic solution,

$$V(t) = \left\{\left[\frac{1}{V_0} + \frac{H\sigma_e}{\dot{\tau}_r}\right]\left[exp\left(\frac{-\dot{\tau}_r t}{a\sigma_e}\right)\right] - \frac{H\sigma_e}{\dot{\tau}_r}\right\}^{-1} \quad (\dot{\tau}_r \neq 0), \qquad (5)$$

where V_0 is the initial slip velocity and $H = b/L - k/\sigma_e$ consists of model constants. The time to instability, t_i, is obtained by substituting a critical slip velocity V_i defining the start of instability into Eq. (5) as

$$t_i(V_0) = \frac{a\sigma_e}{\dot{\tau}_r}\left[ln\left(\frac{1}{V_0} + \frac{H\sigma_e}{\dot{\tau}_r}\right) - ln\left(\frac{1}{V_i} + \frac{H\sigma_e}{\dot{\tau}_r}\right)\right] \sim \frac{a\sigma_e}{\dot{\tau}_r}ln\left(\frac{\dot{\tau}_r}{H\sigma_e V_0} + 1\right). \qquad (6)$$

By taking sufficiently large V_i, $1/V_i$ is negligible in Eq. (6). Time to instability is then calculated for each nucleation source as a function of its V_0. When a constant background seismicity $r = dn/dt$ (events/unit time) is chosen as the reference, corresponding distribution of initial slip velocities over the population of patches is obtained by equating Eq. (6) with the time of the n-th earthquake $t = n/r$ and by rearranging it for initial slip velocity of each patch as

$$V(n) = \left\{\left[\frac{H\sigma_e}{\dot{\tau}_r}\right]\left[exp\left(\frac{\dot{\tau}_r n}{a\sigma_e r}\right) - 1\right]\right\}^{-1} \quad (\dot{\tau}_r \neq 0). \qquad (7)$$

This distribution gives an even interval $\dot{\tau}_r/(a\sigma_e r)$ in log-velocity for each neighboring patches except for the patches (with small n) that have already come close to failure. This can be translated into the distribution of strength excess $\Phi(n) - \tau(n)$ with an essentially even interval of $\dot{\tau}_r/r$, an intuitively understandable feature of the distribution. Because slip velocity increases as the nucleation process proceeds, the distribution of slip velocities on patches evolves with time. However, it has turned out that the distribution of Eq. (7) remains stationary under constant-rate stressing.

When a stress step $\Delta\tau$ is additionally considered, the slip velocity of each patch is instantaneously increased by

$$\Delta V = \Delta\tau \cdot (V/(a\sigma_e)), \qquad (8)$$

(from Eq. (1) with $\Delta\Phi = 0$ because of no slip weakening) and the subsequent acceleration process follows the time to instability obtained by substituting $V_0 = V + \Delta V$ to Eq. (6). Since Eq. (6) is a monotonically decreasing function of V_0, a positive stress step leads to clock advancement for all nucleation sources (Gomberg et al., 1998). The clock advancement

$$\Delta t_{adv}(V, \Delta V) = t_i(V) - t_i(V + \Delta V) \qquad (9)$$

depends on the V of each patch at the moment of stress step. Hence, a temporal change of seismicity follows a stress step unless the curve $t_i(V)$ is linear. If it is convex upward as is the case for Eq. (6), a period of increased seismicity will follow the positive stress step. For the specific functional form of Eq. (6), the altered seismicity $R(t)$, which is defined by the number of patches reaching the instability velocity V_i per unit time, is obtained as

$$R(t) = r \cdot \left\{\left[exp\left(\frac{-\Delta\tau}{a\sigma_e}\right) - 1\right]exp\left(\frac{-t}{t_a}\right) + 1\right\}^{-1}. \qquad (10)$$

As noted in the introduction and Fig. 1, the aftershock rate jumps up to R_0 and begins to decay along the $1/t$ asymptote after the decay onset time t_e, eventually merging to the background rate for $t/t_a > 1$.

3.2. Time-to-instability analysis with the revised RSF

In order to obtain a parallel analytic from of the aftershock rate $R(t)$ with the Nagata RSF, we begin by deriving an analytic solution for the time to instability $t_i(V_0)$. By adopting the same assumption of omitting the time-healing term in the Nagata evolution law (Eq. (3)), we obtain slip velocity history and the time to instability by solving Eq. (4) with the initial slip velocity V_0 as

$$V(t) = \left\{ \left[\frac{1}{V_0} + \frac{H' \sigma_e}{(c+1)\dot{\tau}_r} \right] \left[exp\left(\frac{-(c+1)\dot{\tau}_r t}{a\sigma_e} \right) \right] - \frac{H' \sigma_e}{(c+1)\dot{\tau}_r} \right\}^{-1} \quad (\dot{\tau}_r \neq 0),$$

$$(11)$$

$$t_i(V_0) = \frac{a\sigma_e}{(c+1)\dot{\tau}_r} ln\left(\frac{(c+1)\dot{\tau}_r}{H' \sigma_e V_0} + 1 \right),$$

$$(12)$$

where $H' = b/L - (c+1)k/\sigma_e$ and $1/V_i$ is omitted in Eq. (12). These parallel versions coincide with those for the Dieterich RSF when $c = 0$. By comparing Eqs. (6) and (12), we see relevant changes are only in the coefficients $a^N/(c+1)$ and $(c+1)/H'$ in Eq. (12). When the laboratory-derived parameter sets N-0 and N-2 are substituted, we see that $a^N/(c+1) \sim a^D$ and $(c+1)/H' \sim 1/H$, suggesting that the $R^N(t)$ would be quantitatively very similar to $R^D(t)$. However, this is a wrong conclusion because Eq. (12) is, in fact, not very accurate.

In Fig. 2, the analytic time-to-failure curves, Eq. (6) based on the Dieterich RSF and Eq. (12) based on the Nagata RSF, are compared with the corresponding numerically derived time-to-failure curves obtained without omitting the healing term. The numerical results were derived by Runge–Kutta integration (Press et al., 1992) of Eq. (4) coupled with Eq. (2) or Eq. (3), started with a variety of initial slip velocities. We assumed background loading velocity $V_{pl} = \tau_r/k = 4.5$ cm/year, patch stiffness $k = 5.0$ MPa/m, velocity for instability $V_i = 10^{10} V_{pl} (= 1.4$ m/s), effective normal stress $\sigma_e = 100$ MPa and 10^5 times larger L at a seismogenic depth 10 km as employed in our seismic cycle simulations with the revised RSF (Kame et al., 2013). The chosen k is smaller than the critical stiffness $k_c = (b-a)\sigma_e/(1+c)L$ (Kame et al., 2013; Ruina, 1983), satisfying the unstable condition necessary for nucleation.

The analytic solution does not agree very well to the numerical result in case of the Nagata RSF (Fig. 2b), contrasting to the excellent agreement in case of the Dieterich RSF (Fig. 2a). The reason should be the large coefficient of time-healing term b/L in the Nagata RSF; b^N/L^N is five times greater than b^D/L^D. Though not presented, we actually proceeded to obtain $R^N(t)$ using the numerical time-to-failure curve for the Nagata RSF (solid line in Fig. 2b), which did differ somewhat from the following (wrong) $R^N(t)$ obtained using the (wrongly approximated) analytic time-to-instability function (Eq. (12), dashed line in Fig. 2b):

$$R(t)^N = r \cdot \left\{ \left[exp\left(\frac{-(c+1)\Delta\tau}{a\sigma_e} \right) - 1 \right] exp\left(-\frac{t}{t'_a} \right) + 1 \right\}^{-1} \quad \left(t'_a = \frac{a\sigma_e}{(c+1)\dot{\tau}_r} \right).$$

$$(13)$$

At that point, we decided to switch to a fully numerical approach to obtain seismicity directly by recording the time of instability of each nucleation source that was numerically simulated using full RSF. We describe the method in Section 3.3 and discuss the result in Section 4, including a finding of another (and deeper) pitfall still overlooked in the discussion of time-healing term above.
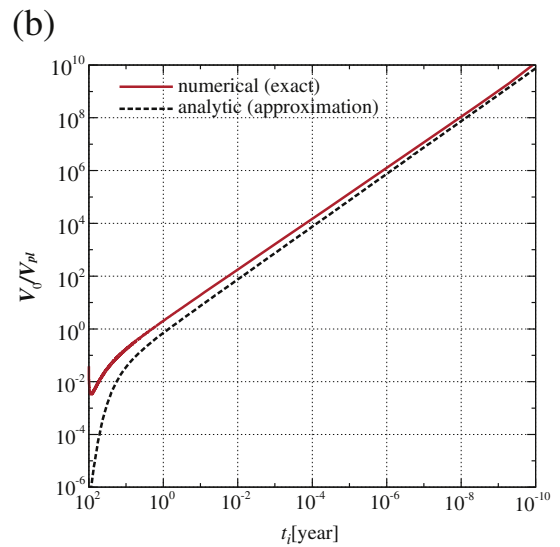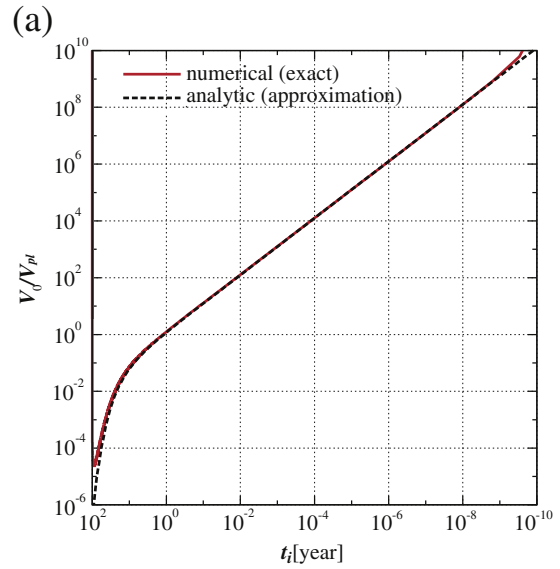

(a)

(b)

Fig. 2. Comparison between numerical (solid line) and analytic (dashed line) solutions of time-to-instability analysis. (a) Case with the Dieterich RSF. (b) Case with the Nagata RSF.

3.3. Aftershock triggering model: Numerical approach

We employ an alternative numerical approach in deriving the aftershock triggering sequence $R(t)$ obeying the Nagata RSF. As Gomberg et al. (2005) did, we shall track the slip history of each fault until seismic instability occurs under loading conditions where a stress step is superimposed at a time $t = t_M$ on the sustained tectonic loading at a constant rate.

In Dieterich (1994), the time to instability $t_i(V_0)$ is connected with the constant reference seismicity r to give the stationary distribution of slip velocities on patches $V(n)$. Then stress step loading $\Delta\tau$ raises the velocity of each patch by $\Delta V = \Delta\tau \cdot (V/(a\sigma_e))$, and subsequent acceleration processes follow the time to instability $t_i(V + \Delta V)$. Because $t_i(V + \Delta V) < t_i(V)$ in Eq. (6), the time of instability is always advanced by a positive stress step. Because the clock advance Δt_{adv} decreases with $V(n)$, a temporal increase of aftershock rate $R(t)$ occurs. The greatest contribution to the rate increase comes from the population of the faults that had been closest to failure at the time of stress step $t = t_M$ (Gomberg et al., 2005). In our numerical approach, we exactly consider individual n nucleation patches on which identical initial

steady state values, (V_0, Φ_0, τ_0), are assumed. Under this initial condition, we began constant-rate loading of each patch at timings different by an even interval Δt so that instability of each patch will occur with the same interval Δt. Obviously, this will result in the constant seismicity rate $r = 1/\Delta t$. Then we additionally consider a stress step $\Delta \tau$ at $t = t_M$ simultaneously on all patches. Remotely applied loading function for the k-th patch is thus given by

$$\tau^k(t) = \tau_0 + \dot{\tau}_r \cdot (t - t_k) \cdot H(t - t_k) + \Delta \tau \cdot H(t - t_M) \qquad (k = 1, ..., n), \quad (14)$$

where $t_k = k\Delta t$. We numerically solve Eqs. (4) and (3) under the loading condition Eq. (14) and the initial condition (V_0, Φ_0, τ_0) by using a Runge–Kutta method. Fig. 3 schematically shows the loading history on the k-th patch (top) and the resultant slip velocity histories of many patches (bottom). It must be noted that the initial slip velocity V_0 does not alter simulation results as long as it is much smaller than the characteristic loading velocity V_{pl} appearing in the background stressing rate $\dot{\tau}_r (= V_{pl} \cdot k)$. By simulating all nucleation processes controlled by the applied load in Eq. (14), the onset time series of triggered events are determined. Then the aftershock rate $R(t)$ is given by the number of events per every unit time after t_M.

In the following aftershock simulations, we assume background loading velocity $V_{pl} = \dot{\tau}_r/k = 4.5$ cm/year, effective normal stress $\sigma_e = 100$ MPa at depth, initial steady-state slip velocity $V_0 = 10^{-6} V_{pl}$, instability velocity $V_i = 0.1$ m/s ($\sim 10^8 V_{pl}$) and $n = 10^5$ patches in total. The characteristic length scale is $L^{sim} = 10^2 L$ instead of $L^{sim} = 10^5 L$ assumed to simulate the cycle of large earthquakes (Kame et al., 2013). Correspondingly, patch stiffness $k = 500$ MPa/m is chosen so that unstable

self-accelerating slip condition $k/k_c < 1$ is realized on patches ($k/k_c^D = 0.057$ and $k/k_c^N = 0.090$). Note that different L does not alter the results below as long as k/k_c is kept the same.

4. Result

4.1. Stress-step responses obeying RSF

Here we examine a slip response following a stress step $\Delta \tau$ in detail. We compare cases with the Dieterich RSF (N-0) and the Nagata RSF (N-2). The slip velocity increment with the Nagata RSF is obtained as

$$\Delta V = \Delta \tau \cdot (c + 1) V/(a\sigma_e), \qquad (15)$$

by considering the instantaneous state change ($\Delta \Phi = -c \cdot \Delta \tau$ from the Nagata evolution law, Eq. (3)) in Eq. (1). Two parameter sets N-0 and N-2 lead to quantitatively the same velocity changes ΔV^D and ΔV^N because a^D and $a^N/(c+1)$ becomes equal for these parameter values. As discussed in Section 3.2, the increased velocity always advances the time of instability in the case of the Dieterich RSF. However, we here show that this is not always the case with the Nagata RSF. To our surprise, earthquake timing can be sometimes delayed instead of advanced, depending on the timing of imposed stress step.

The two cases are illustrated in Fig. 4. The broken line (Case 1) is the "ordinary" response where the instantaneous velocity increase ΔV upon the step loading is followed by further monotonic acceleration towards seismic instability. All the simulations with N-0 and
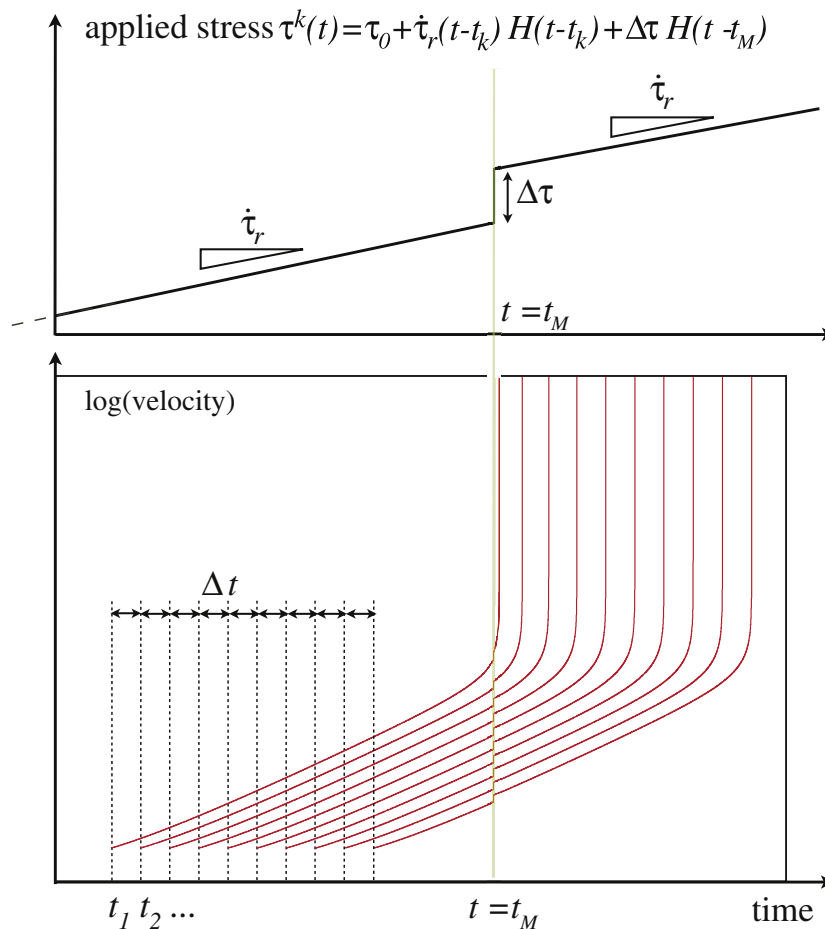

applied stress $\tau^k(t) = \tau_0 + \dot{\tau}_r(t - t_k) H(t - t_k) + \Delta \tau H(t - t_M)$
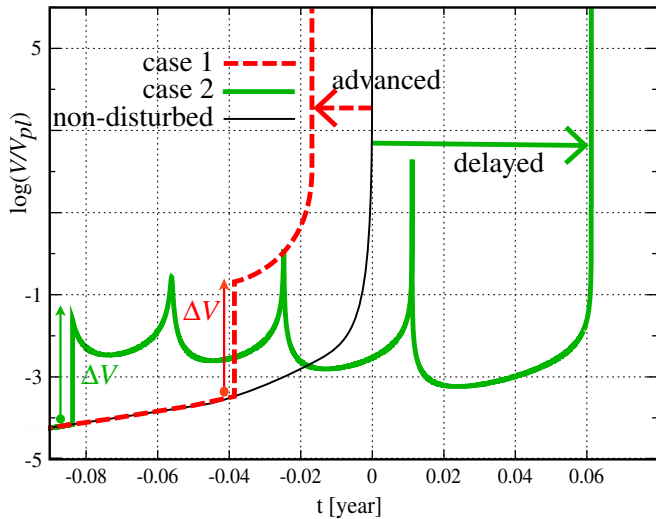
Fig. 3. Schematic illustration of the loading history on the k-th patch, where a sudden stress step at $t = t_M$ is superimposed on the sustained loading at a constant rate $\dot{\tau}_r$ (upper panel) and corresponding slip velocity histories on many patches (lower panel).

Fig. 4. Two contrasting responses (schematic) against a positive step loading imposed at different timings in the seismic cycle driven by constant-rate loading. Thin solid line represents the reference case without step loading. Broken line (Case 1) shows a straightforward response of further monotonic acceleration toward instability, resulting in the advanced timing of the earthquake. Thick solid line (Case 2) shows a peculiar response where the earthquake timing is delayed by extra oscillatory cycles of slow slip events.

the great majority of the simulations with N-2 produced this straightforward behavior. This type of response necessarily advances the timing of earthquake. In contrast, the response indicated by the thick solid line (Case 2) looks very bizarre. The instantaneous velocity increase upon the step loading is immediately followed by a velocity decrease. Though this case also eventually ends up with seismic instability, several oscillatory cycles with an increasing amplitude are experienced before the eventual earthquake, and the timing of earthquake can be delayed from what would have been the case if there were no stress step. This type of behavior was found for simulations with N-2 when a sufficiently large stress step was imposed at a certain range of timing in the spontaneous nucleation path (thin solid line) under the constant stressing rate.

In order to understand the peculiar "Case 2" response of Fig. 4, we plot the behavior in the (V,τ) phase diagram in Fig. 5. The solid line shows the trajectory of "non-disturbed" nucleation under constant-rate loading. Either in the Dieterich RSF case (Fig. 5a) or the Nagata RSF (Fig. 5b) case, V first increases with an increasing shear stress τ along the approximately constant positive inclination a^D or a^N. This implies that Φ is approximately constant in this "locked stage" ($V < V_{pl}$) of the earthquake cycle. After V exceeds the loading velocity, V increases with a decreasing τ, which implies that Φ is decreased by slip-weakening in this "self-accelerating stage" ($V > V_{pl}$). These tendencies in the locked and self-accelerating stages have been well known in earthquake cycle simulations with RSF (e.g., Kato and Tullis, 2003).

When a stress step $\Delta\tau$ is applied to a fault evolving along the non-disturbed line, both velocity and stress instantaneously jump up to a "landing point" $(V',\tau')=(V+\Delta V,\tau+\Delta\tau)$. Subsequent behavior is determined by the position of the landing point in the phase diagram. If the stress step is applied during the self-accelerating stage, the landing point is always above the non-disturbed line. Hence, subsequent behavior is further monotonic acceleration to seismic instability (Rice and Gu, 1983). The time-to-instability analyses shown in Fig. 2 only covered this range of initial conditions and hence showed innocuous monotonic curve for both the Dieterich and Nagata RSFs, pretending that nothing drastic would happen.

However, if the stress step is applied during the locked stage as exemplified by the dashed lines in Fig. 5, a drastically different
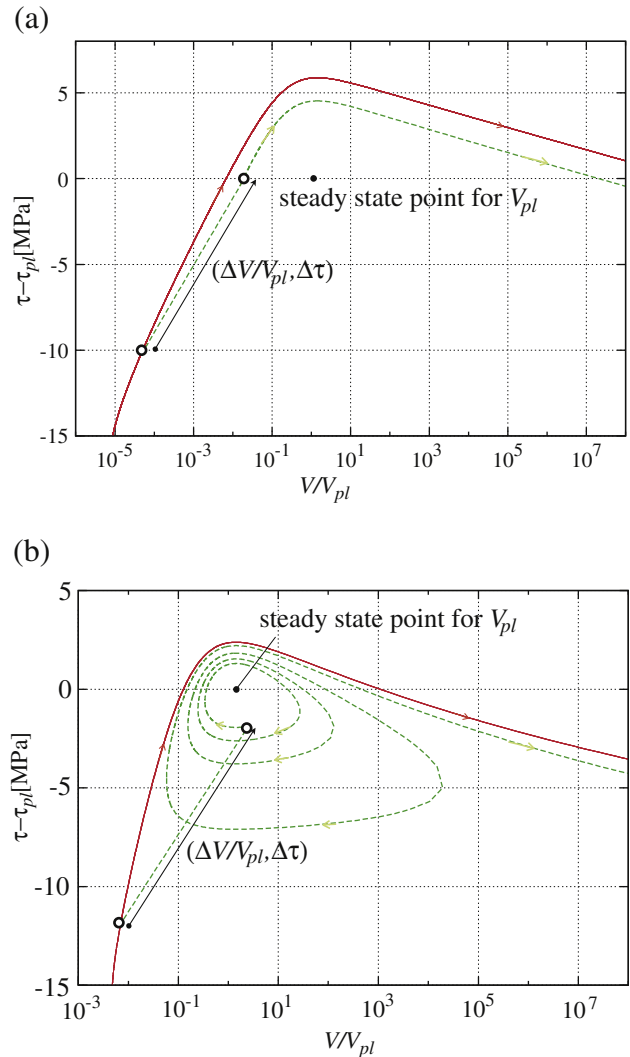
Fig. 5. Phase diagrams of simulated slip responses following a stress step $\Delta\tau = 10$ MPa (dashed line). Solid line shows the "non-disturbed" evolution under the background constant-rate stressing. (a) A case with the Dieterich RSF. (b) A case with the Nagata RSF.

outcome is possible for the Nagata RSF. Noticing that the jump is along the constant-state line in the Dieterich RSF, and also noticing that the non-disturbed evolution (solid line) in the locked stage is nearly along the constant-state line, we can expect that the landing point is close to the non-disturbed line. Hence, subsequent behavior can be reasonably approximated by following the non-disturbed line starting with $V_0 = V'$, as reviewed in Section 3.2. Strictly saying, the landing point is somewhat off the non-disturbed line even for the Dieterich RSF as seen in Fig. 5a, but is still close enough to it so that subsequent behavior is further monotonic acceleration toward seismic instability (dashed line in Fig. 5a). Although we do not rule out the possibility to find a narrow range of conditions to make the Dieterich RSF behave otherwise, at least nothing peculiar happened in our simulations including many trials not presented here. In contrast, with the Nagata RSF (Fig. 5b), the jump is not along the constant-state line at all, due to the instantaneous state change by the stress-weakening effect. Hence the landing point (V',τ') can be significantly below the non-disturbed line and can be sufficiently close to the steady-state sliding point $(V_{pl},\tau_{ss}(V_{pl}))$. When this happens, the following evolution will go along an expanding spiral orbit, sometimes requiring several oscillatory cycles before reaching seismic instability (dashed line in Fig. 5b). Timing of the earthquake is delayed in this case.

On the other hand, if the stress step is applied for faults with velocities much slower than $V_{pl}(=1.4 \times 10^{-9})$ m/s, say, $V < 10^{-6} V_{pl}$ m/s, the landing point is far enough from the steady-slinging point to proceed directly to instability without spiraling. Thus, only for the intermediate stage somewhat before the self-acceleration period of the seismic cycle, step loading can cause the peculiar oscillation and delay the time of earthquake.

In the following subsection, we will see how these "advanced" and "delayed" time of instability affect the resultant aftershock seismicity $R(t)$ obeying the Nagata RSF.

4.2. Simulated aftershock sequences

We conduct aftershock triggering simulations with the Dieterich RSF (N-0) and the Nagata RSF (N-2). We adopt $\Delta\tau = 2.0$, 4.0, 6.0, 8.0, 10 MPa corresponding to the characteristic stresses $a^D\sigma_e = 1.7$ MPa, or $a^N\sigma_e = 5.1$ MPa. These $\Delta\tau$ values may seem to be too large for stress interaction due to a main shock whose typical stress drop is about 5 MPa, but the ratios $\Delta\tau/(a\sigma_e)$ in the simulations are comparable to those usually used to fit the observed seismicity with $\Delta\tau = 0.1 \sim 0.5$ MPa and $a\sigma_e = 0.05$ MPa.

Fig. 6a shows the aftershock seismicity obtained by our numerical approach with the Dieterich RSF. Each curve was indistinguishable from analytic solution Eq. (10), though not shown in the figure. The agreement fully confirms the validity of the Dieterich's (1994) analytic result in the case of the Dieterich RSF. Following the instantaneous activation to R_0^D, the seismicity turned to decay along the $1/t$ asymptote and eventually merged to the background rate at $t_a^D = (a^D\sigma_e/\dot{\tau}_r \sim 660$ hours).

Fig. 6b shows the results with the Nagata RSF also obtained by our numerical approach. In general, the initial seismicity rate R_0^N is higher than the case with the Dieterich RSF for the same $\Delta\tau$. In our numerical simulation, R_0 is defined at $t = 10^0$ hour, the minimum discretized time for the assumed time interval $\Delta t = 10^0$ hours in the background seismicity (Eq. (14)). For quantitative comparison, the normalized initial rates R_0^D/r and R_0^N/r, and their ratio R_0^D/R_0^N for each stress step are summarized in Table 1. The ratio R_0^N/R_0^D tends to be larger for larger $\Delta\tau$. It becomes 2.2 for the largest loading $\Delta\tau = 10.0$ MPa. The onset time of aftershock decay, t_e, is shorter for the Nagata RSF (Fig. 6). These minor improvements can be attributed to the modest difference in time-to-instability curves based on the Dieterich RSF (solid line in Fig. 2a) and the Nagata RSF (solid line in Fig. 2b). Note that both t_e and R_0 represent the initial part of an aftershock sequence and hence are essentially governed by the behaviors of nucleation sources that were already in the self-accelerating stage at the time of main shock, which is well summarized by Fig. 2. The Nagata RSF has thus narrowed the two known gaps between the RSF triggering model and common aftershock observations. However, the both improvements are only by a factor, far from the orders-of-magnitude gaps to be mediated. The problem is still there essentially to the same extent.

Other potentially important differences have been made by the Nagata RSF. Firstly, the Nagata RSF can produce the time-decay exponent p larger than unity, which increases with $\Delta\tau$ (Fig. 6b), contrasting that p is fixed at unity with the Dieterich RSF (Dieterich, 1994). In our simulations, p increased from 1.0 to 1.8 as $\Delta\tau$ increased from 2.0 to 10.0 MPa (Fig. 6b). Implications will be discussed in Section 5. Secondly, aftershock rate $R^N(t)$ decreases once below the background rate and then increases back to r (Fig. 6b), whereas $R^D(t)$ monotonically decreases to r (Fig. 6a). The overshoot is more emphasized for greater $\Delta\tau$ (Fig. 6b). Thirdly, the aftershock duration t_a^N has $\Delta\tau$ dependency, whereas the Dieterich RSF produces a constant t_a^D independent of $\Delta\tau$. Significant shortening to $t_a^N = 200$ hours is found for $\Delta\tau = 10.0$ MPa, which is about 30% of the prediction $t_a^D = 660$ hours by the Dieterich RSF. Again, the shortening effect is more significant for greater $\Delta\tau$.
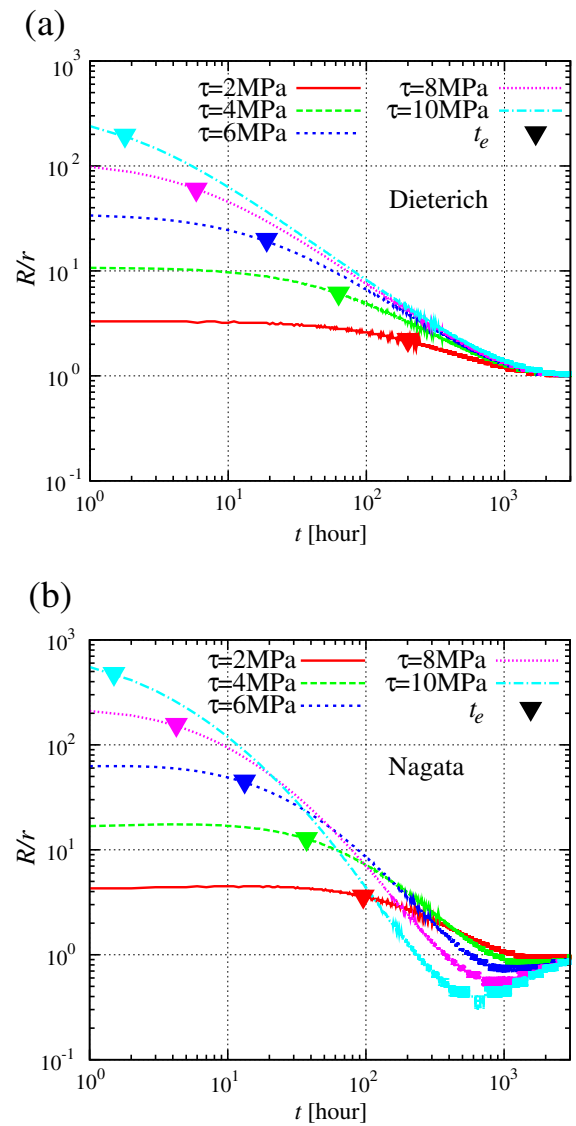
Fig. 6. Simulated seismicity following five different stress steps. (a) Results with the Dieterich RSF. (b) Results with the Nagata RSF. The theoretical prediction of t_e in the Dieterich and our graphical interpretation of the timing of t_e in the Nagata (the intersection of $R/r = R_0(= \text{const.})$ and tangent line to each decaying curve) are marked with triangles. t_a is not marked here. From the theoretical prediction t_a^D is constant (~ 660 hours), whereas t_a^N, the time returning to $R/r = 10^0$ numerically determined, varies with $\Delta\tau$.

These three interesting features all resulted from the delayed earthquake timing for population with intermediate V at $t = t_M$, which follows the clock-advanced population with highest V at $t = t_M$ that produced the higher R_0 and the shorter t_e. As mentioned in Section 4.1, the initial sudden increase of seismicity comes from nucleation sources that were very close to instability at the time of mainshock. They were already in the self-accelerating period and the time of instability was advanced. The population next up was in

Table 1
Stress Step and Simulation Results.

$\Delta\tau$ [MPa]	R_0^D/r	R_0^N/r	R_0^N/R_0^D
2.0	3.2	4.2	1.3
4.0	10	17	1.7
6.0	34	64	1.9
8.0	97	211	2.2
10.0	243	539	2.2

the locked stage somewhat before entering the self-accelerating stage, for which the "delayed" time of instability can occur. This transition from the clock-advanced to clock-delayed population resulted in the rapid time decay of $R^N(t)$, which also manifested as (i) the large $p > 1$, (ii) the temporal drop of seismicity below the background rate and (iii) the short t_a^N, defined by the time when $R^N(t)$ first came back to r. Because the importance of clock-delayed population depends on the amount of stress step $\Delta\tau$, these features necessarily have stress step dependences. After consuming clock-delayed population, another clock-advanced population with lowest initial velocities at t_M comes into action, raising the seismicity back to the background level. This is because the sources with very low slip velocities were subjected to essentially the same amount of time advancement, keeping the time interval between events unchanged at the $\Delta\tau$ set originally.

5. Discussion

On the way to obtain the aftershock triggering model with the Nagata RSF through our fully numerical approach, we noticed an unanticipated slip response detailed in Section 4.1; an imposed positive stress step drives the system toward stability and delays the timing of the earthquake on the receiver fault, introducing extra slow slip events before reaching eventual instability. This is no more only a matter of aftershock triggering mechanism, but represents a new possibility in fundamental behavior of earthquake cycles. The behavior implies that a fault at a stage somewhat before entering the self-accelerating stage can be marked by a characteristic response of repeated slow slip events with a short interval.

Though it initially looked very bizarre to us, we now know that it is at least understandable on the phase diagram and is directly rooted in the stress-weakening effect, an essential feature of the Nagata RSF. We note that all the significant differences made by the Nagata RSF on the aftershock triggering were through this counterintuitive effect. However, the behavior has not been directly confirmed by laboratory experiments. Laboratory friction tests specifically designed to reproduce this behavior are desired.

Omori–Utsu law is a well-established empirical formula describing time-decay of aftershock rate. From observations, the exponent p is typically 1, with some variations from case to case, whereas the Dieterich RSF predicts $p = 1$, not depending on the parameter values or the imposed $\Delta\tau$. If the numerically derived slow slip behavior is experimentally confirmed, it may be worth looking for a systematic dependence of p on $\Delta\tau$ as suggested by the Nagata RSF. The prediction of $p > 1$ by the Nagata RSF may look inconsistent with the observation of $p = 1$ on average. However, this is not true because the type of theoretical triggering models treated in the present paper must be regarded as a "bare triggering kernel," which does not consider the cascade of triggering, i.e., aftershocks of aftershocks and so on (e.g., ETAS in Ogata, 1988). Such cascading should necessarily result in an extended tail in aftershock decay, making the directly observed p somewhat smaller than that of the bare kernel. In fact, analysis for p of bare kernel from natural aftershock sequences has found p as large as 1.4 (Felzer et al., 2003; Marsan and Lengline, 2008).

6. Conclusion

Motivated by the existing discrepancies between the model predictions of Dieterich (1994) and the observed aftershock seismicity, we re-examined aftershock triggering on faults obeying the recently revised RSF (Nagata et al., 2012) that seems eventually free from contradictions with laboratory friction experiments. Time-to-instability analysis, which is necessary as a specific nucleation model to get on the original theoretical framework of Dieterich's aftershock modeling, found that the assumption of omitting time-healing term in the analysis is not precise enough for the Nagata RSF. We thus employed an alternative numerical approach. We simulated the nucleation process of individual faults in the population subjected to a step increase in stress and counted the number of triggered events per unit time to obtain the aftershock rate as a function of time after the mainshock. Our results showed certain improvements towards common observations, in terms of raised seismicity and shortened delay before Omori decay. However, the improvements were far too small to resolve the huge quantitative gap in the characteristic stress $a\sigma_e$ between laboratory values and what is inferred from observed aftershock sequences. On the other hand, through many numerical simulations of slip response to a stress step imposed at different timings in the seismic cycle, we noticed a counterintuitive behavior of the Nagata RSF. When a sufficiently large stress step is imposed at a timing somewhat before entering self-accelerating stage of the seismic cycle, the timing of earthquake can be delayed rather than advanced. In this case, the earthquake will occur after several oscillatory cycles resembling slow slip events, which might be usable as a marker for a fault at a certain stage in the seismic cycle. This behavior itself is a potentially important finding in earthquake mechanics, but also has some consequences on aftershock triggering. Firstly, predicted time-decay exponent p can be significantly larger than unity, increasing with the stress step induced by the main shock. This may be a good thing, considering that the commonly observed $p \sim 1$ must be somewhat lower than the p of the bare triggering kernel predicted by this kind of modeling where cascades of triggering are not considered. Secondly, aftershock decay, especially for a larger step increase in the stress field, may once overshoot below the background seismicity. These effects combinedly produce a negative dependence of aftershock duration on the imposed stress step. With these interesting predictions, a laboratory confirmation of the counterintuitive response of a frictional fault to a stress step, which is an unintended prediction by the Nagata RSF, is desired.

References

Ampuero, J.P., Rubin, A.M., 2008. Earthquake nucleation on rate and state faults—aging and slip laws. Journal of Geophysical Research 113 (B01302) http://dx.doi.org/10.1029/2007JB005082.
Beeler, N.M., Tullis, T.E., Weeks, J.D., 1994. The roles of time and displacement in the evolution effect in rock friction. Geophysical Research Letters 21, 1987–1990.
Cochran, E.S., Vidale, J.E., Tanaka, S., 2004. Earth tides can trigger shallow thrust fault earthquakes. Science 306, 1164–1166.
Dieterich, J.H., 1979. Modeling of rock friction 1. Experimental results and constitutive equations. Journal of Geophysical Research 84, 2161–2168.
Dieterich, J.H., 1992. Earthquake nucleation on faults with rate- and state-dependent strength. Tectonophysics 211, 115–134.
Dieterich, J.H., 1994. A constitutive law for rate of earthquake production and its application to earthquake clustering. Journal of Geophysical Research 99, 2601–2618.
Dieterich, J.H., Kilgore, B.D., 1996. Imaging surface contacts: power law contact distributions and contact stresses in quartz, calcite, glass and acrylic plastic. Tectonophysics 256, 219–239.
Dieterich, J.H., Cayol, V., Okubo, P., 2000. The use of earthquake rate changes as a stress meter at Kilauea volcano. Nature 408, 457–460.
Felzer, K.R., Rachel, E.A., Ekstrom, G., 2003. Secondary aftershocks and their importance for aftershock forecasting. Bulletin of the Seismological Society of America 93, 1433–1448.
Gomberg, J., Beeler, N.M., Blanpied, M.L., Bodin, P., 1998. Earthquake triggering by transient and static deformations. Journal of Geophysical Research 103, 24411–24426.
Gomberg, J., Reasenberg, P., Cocco, M., Belardinelli, M.E., 2005. A frictional population model of seismicity rate change. Journal of Geophysical Research 110 (B05S03) http://dx.doi.org/10.1029/2004JB003404.

Gross, S., Kisslinger, C., 1994. Estimating tectonic stress rate and state with Landers aftershocks. Journal of Geophysical Research 102 (B4), 7603–7612.

Kame, N., Fujita, S., Nakatani, M., Kusakabe, T., in preparation. Earthquake nucleation on faults with a revised rate- and state-dependent friction law. Geophys. Res. Lett.

Kame, N., Fujita, S., Nakatani, M., Kusakabe, T., 2013. Earthquake cycle simulation with a revised rate- and state-dependent friction law. Tectonophysics 600, 196–204.

Kato, N., Tullis, T.E., 2001. A composite rate- and state-dependent law for rock friction. Geophysical Research Letters 28, 1103–1106.

Kato, N., Tullis, T.E., 2003. Numerical simulation of seismic cycles with a composite rate- and state-dependent friction law. Bulletin of the Seismological Society of America 93, 841–853.

Lohman, R.B., McGuire, J.J., 2007. Earthquake swarms driven by aseismic creep in the Salton Trough, California. Journal of Geophysical Research 112 (B04405) http://dx.doi.org/10.1029/2006JB004596.

Marone, C., 1995. Fault zone strength and failure criteria. Geophysical Research Letters 22, 723–726.

Marsan, D., Lengline, O., 2008. Extending earthquakes' reach through cascading. Science 319, 1076–1079 http://dx.doi.org/10.1126/science.1148783.

Nagata, K., Nakatani, M., Yoshida, S., 2012. A revised rate- and state-dependent friction law obtained by constraining constitutive and evolution laws separately with laboratory data. Journal of Geophysical Research 117 (B02314) http://dx.doi.org/10.1029/2011JB008818.

Nakatani, M., 2001. Conceptual and physical clarification of rate and state friction: frictional sliding as a thermally activated rheology. Journal of Geophysical Research 106, 13347–13380.

Ogata, Y., 1988. Statistical models for earthquake occurrences and residual analysis for point processes. Journal of the American Statistical Association 83, 9–27.

Omori, F., 1894. On the aftershocks of earthquakes. Journal of the College of Science, Imperial University of Tokyo 7, 111–200.

Press, W.H., Teukolsky, S.A., Vetterling, W.T., Flannery, B.P., 1992. Numerical Recipes, 2nd. ed. Cambridge Univ. Press, New York.

Rice, J.R., Gu, J.C., 1983. Earthquake aftereffects and triggered seismic phenomena. Pure and Applied Geophysics 121, 187–219.

Ruina, A., 1983. Slip instability and state variable friction laws. Journal of Geophysical Research 88, 10359–10370.

Scholz, C.H., 2002. The Mechanics of Earthquakes and Faulting, 2nd ed. Cambridge University Press, Cambridge.

Segall, P., Desmarais, E., Shelly, D., Miklius, A., Cervelli, P., 2006. Earthquakes triggered by silent slip events on Kilauea volcano, Hawaii. Nature 442, 71–74.

Toda, S., Stein, R.S., Reasenberg, P.A., Dieterich, J.H., 1998. Stress transferred by the Mw = 6.5 Kobe, Japan, shock: effect on aftershocks and future earthquake probabilities. Journal of Geophysical Research 103, 24543–24565.

Toda, S., Stein, R.S., Dinger, K.R., Bozkurt, S.B., 2005. Forecasting the evolution of seismicity in southern California: animations built on earthquake stress transfer. Journal of Geophysical Research 110 (B05S16) http://dx.doi.org/10.1029/2004JB003415.

Tse, S.T., Rice, J.R., 1986. Crustal earthquake instability in relation to the depth variation of frictional slip properties. Journal of Geophysical Research 91, 9452–9472.

Utsu, T., 1961. A statistical study of the occurrence of aftershocks. Geophysical Magazine 30, 521–605.

Weeks, J., 1993. Constitutive laws for high-velocity frictional sliding and their influence on stress drop during unstable slip. Journal of Geophysical Research 98, 17,637–17,648.

Yoshida, S., Kato, N., 2003. Episodic aseismic slip in a two-degree-of-freedom block-spring model. Geophysical Research Letters 30 http://dx.doi.org/10.1029/2003GL017439.